High-Entropy Alloys in Hexagonal Close-Packed Structure

M.C. GAO, B. ZHANG, S.M. GUO, J.W. QIAO, and J.A. HAWK

The microstructures and properties of high-entropy alloys (HEAs) based on the face-centered cubic and body-centered cubic structures have been studied extensively in the literature, but reports on HEAs in the hexagonal close-packed (HCP) structure are very limited. Using an efficient strategy in combining phase diagram inspection, CALPHAD modeling, and *ab initio* molecular dynamics simulations, a variety of new compositions are suggested that may hold great potentials in forming single-phase HCP HEAs that comprise rare earth elements and transition metals, respectively. Experimental verification was carried out on CoFeReRu and CoReRuV using X-ray diffraction, scanning electron microscopy, and energy dispersion spectroscopy.

DOI: 10.1007/s11661-015-3091-1

I. INTRODUCTION

THE core concept of high-entropy alloys (HEAs)[1,2] is to maximize the configurational entropy of solid solution phases *via* equi-molar compositions among multi-principal elements (for a comprehensive review, see References 3, 4). To date, there are very limited single-phase HEAs reported, and arbitrary mixing of four or more principal elements at equi-molar compositions usually does not render formation of disordered solid solutions.[1,5–7] This has posed great difficulty in understanding HEA formation mechanisms or establishing HEA formation rules (for a recent review in this topic, see Reference 8). The vast majority of reports pertaining to HEAs are focused on face-centered cubic (FCC) structures, body-centered cubic (BCC) structures, or their mixtures. Early work on FCC HEAs is based on CoCrFeMnNi[1] and its derivatives such as CoCrFeNi,[9] CoFeMnNi,[5,10] and CoCrMnNi,[10] and excessive addition of BCC stabilizers such as Al to them causes the formation of BCC and/or ordered BCC (*i.e.*, CsCl-type B2) structures.[11–14] Recently, by inspecting phase diagrams and performing *ab initio* molecular dynamics (AIMD) simulations, Gao and Alman[5] suggested new single-phase FCC HEAs based on noble metals including CuNiPdPtRh and CuNiPdPt. Other BCC HEAs reported in the literature are centered on refractory metals.[15–19]

In contrast, the progress in the design and fabrication of the hexagonal close-packed (HCP) HEAs has been slow. Chen *et al.*[20] prepared BeCoMgTi and BeCoMgTiZn alloys that are entirely composed of HCP elements using mechanical milling, but no crystalline solid solutions and compounds formed before full amorphization. Detailed analysis on the formation of HCP HEAs was performed by Zhang *et al.*[3] who stated that the difficulty in forming HCP HEAs was because most elements in the periodic table prefer a BCC or FCC structure. Elements Cd, Mg, Os, Re, Ru, Tc, and Zn possess only one stable structure in HCP lattice below their melting points, while Be, Sc, Ti, Zr, and Hf transfer from the HCP to BCC structure and Co from the HCP to FCC structure at high temperatures. While HCP CoOsReRu HEA was suggested in Reference 5, Youssef *et al.*[21] reported that $Al_{20}Li_{20}Mg_{10}Sc_{20}Ti_{30}$ transformed from FCC to HCP structure after annealing at 773 K (500 °C) for 1 hour. However, it is not known whether the FCC and HCP phases formed in $Al_{20}Li_{20}Mg_{10}Sc_{20}Ti_{30}$ are thermodynamically stable.

On the other hand, most rare earth elements have an HCP or double HCP (*i.e.*, DHCP, Pearson symbol hP4, space group $P6_3/mmc$) structure that is stable over wide temperature ranges below their melting points. Because of the extreme similarity in atomic size, electronegativity, and chemistry, most of them form isomorphous or extended solid solution in the HCP or DHCP structure according to their binary phase diagrams.[22] Therefore, for the first time, Zhang *et al.*[3] proposed the likelihood of forming single-phase HCP HEAs based on rare earth elements. Indeed, the formation of HCP HEAs was later confirmed in DyGdHoTbY,[23] DyGdLuTbY,[24] and DyGdLuTbTm.[24] Note that the X-ray diffraction (XRD) pattern was not provided for DyGdHoTbY[23] and was not indexed for DyGdLuTbY[24] and DyGdLuTbTm.[24]

Motivated by the scarcity of single-phase HCP HEAs in the literature, the objective of the present study was to accelerate HCP HEA design using the efficient searching scheme proposed in Reference 5 by combining phase diagram inspection, CALPHAD (acronym of CALculation

M.C. GAO, Principal Materials Scientist, is with the AECOM at National Energy Technology Laboratory, P.O. Box 1959, Albany, OR 97321. Contact e-mail: michael.gao@netl.doe.gov B. ZHANG, Graduate Student, and S.M. GUO, Professor, are with the Department of Mechanical & Industrial Engineering, Louisiana State University, Baton Rouge, LA 70803. J.W. QIAO, Professor, is with the Department of Materials Science and Engineering, Taiyuan University of Technology, Taiyuan 030024, China. J.A. HAWK, Group Leader, is with the Structural Materials Development Division, National Energy Technology Laboratory, Albany, OR 97321.

Manuscript submitted May 25, 2015.
Article published online August 28, 2015

of PHAse Diagrams) modeling, and AIMD simulations, which comprise rare earth elements and transition metals, respectively. This searching strategy has led to the recent discovery of senary BCC HEAs of MoNbTaTiVW[16] and HfNbTaTiVZr.[18]

II. COMPUTATIONAL AND EXPERIMENTAL PROCEDURES

A. *Computational Modeling*

CALPHAD calculations were carried out mainly using the TCNI7 thermodynamic database *via* the ThermoCalc™ software[25] on equi-molar compositions CoReRuX, CoPtReRuX, CoFeReRuX, and MoRuPdX, where X refers to the substitutional elements that are covered in the TCNI7 database, *e.g.*, Al, Cr, Hf, Mn, Ni, Ti, V, W, Zr, *etc*. The database covers all the constituent binaries between these elements except Mn-W. SSOL5 database was used for rare earth elements and compositions that contain elements Ir, Os, or Rh.

The AIMD simulations were performed using the plane-wave pseudo-potential software, Vienna Ab Initio Simulation Package (VASP)[26,27] in a canonical ensemble, *i.e.*, constant mole, volume, and temperature. Newton's equations of motion were integrated using the Verlet algorithm[28] with a time step of 1 fs, and the atomic configuration relaxation and temperature were controlled by a Nose thermostat.[29] Projector-augmented wave (PAW) potentials[30] and the revised Perdew–Burke–Ernzerhof[31] gradient approximation to the exchange-correlation functional were used. Cubic supercells of 200 atoms were built for all compositions, and the liquid densities were determined by adjusting the cell volume so that the pressure was zero at equilibrium. The simulations were performed at the Γ point only. A "medium" precision setting, as described in VASP, was used. Spin polarization was not considered. The electronic-energy-convergence criterion was set to 1×10^{-4} eV/at. AIMD simulations were performed at a density of 9.475, 15.119, and 10.155 g/cm^3 with the plane-wave cutoff energy of 155.7, 268.0, and 250.9 eV at 2073 K (1800 °C), 3073 K (2800 °C), and 3073 K (2800 °C) for DyGdLuTbY, CoOsReRu, and MoPdRhRu, respectively, for a total simulation time of more than 30 ps.

The atomic structure in the liquid state can reveal useful information about the preferred interatomic bonding that may impact the formation of disordered solid solution during solidification.[3,5,32] The partial pair distribution function (PDF) gives the information about the probability of such bond formation by measuring the intensity of near-neighbor pairs against the total random distribution, and partial PDF (g_{ab}) was calculated using

$$g_{ab}(r) = \frac{V}{N_a N_b} \frac{1}{4\pi r^2} \sum_{i=1}^{N_a} \sum_{j=1}^{N_b} \langle \delta(|r_{ij}| - r) \rangle, \qquad [1]$$

where V is the volume of the super cell, N_a and N_b are the number of elements a and b, $|r_{ij}|$ is the distance between elements a and b, and the bracket $\langle \ \rangle$ denotes the time average of different configurations. Previous AIMD simulations[3,5,7] show that preferred bond pairs of Al-Ni, Cr-Fe, and Cu-Cu pairs in the liquid $Al_{1.3}$CoCrCuFeNi may serve as the precursors to nucleating B2, BCC, and FCC phases, respectively during solidification. Comparing the PDF among single-phase HEAs, multiphase HEAs, and high-entropy bulk metallic glasses, Zhang *et al.*[5] proposed that a liquid structure that lacks strong elemental segregation or potent short-range order will promote the formation of disordered solid solution during solidification.

Examining the atomic trajectory, the diffusion constants were obtained by plotting the mean square displacement (MSD) *vs* time using the following equation:

$$D_i = \lim_{t \to \infty} \frac{\langle |R_i(t) - R_i(0)|^2 \rangle}{6t}, \qquad [2]$$

where D_i is the self-diffusion constant of species i, and $R_i(t)$ and $R_i(0)$ denote the atomic position of species i at time t and $t = 0$, respectively. The angular brackets denote an average over all the same species.

B. *Alloy Fabrication and Characterization*

Two alloys with a nominal composition of 25 at. pct for each constituent element, namely CoFeReRu and CoReRuV, were prepared using a vacuum arc melting furnace (model Edmund Bühler /MAM-1) under argon atmosphere in a water-cooled copper hearth. The purity of all the raw elemental metal powders is higher than 99.5 wt pct. Before melting, elemental powders were weighed and mixed uniformly in a polystyrene ball mixing jar for 15 minutes. The mixed powders were then melted using an arc melting furnace under Argon gas protection. To enhance the chemical homogeneity, each sample was flipped over and re-melted 3 to 4 times. After the system had cooled to room temperature, the solidified ingots were embedded into an epoxy resin (SamplKwick fast cure acrylic resin, produced by Buehler) for easy handling. A low-speed diamond saw was then used to section the HEA sample to expose a flat surface of the cross section. The exposed surface was subsequently ground using #240, #320, #400, #600, and #800 SiC abrasive papers in sequence, before wet-polished with 1, 0.3, and 0.05 μm Al_2O_3 suspensions. The microstructure was examined in a field-emission scanning electron microscope (FE-SEM) (FEI, Quanta 3DFEG) equipped with back-scatter electron (BSE) and energy dispersion spectroscopy (EDS) detectors. The crystal structures of phases present in the sample were identified using XRD (Empyrean PANalytical) with Cu K_α at a scan rate of 2 deg/minute. The densities of the specimen were determined by weighing the samples and calculating the volume. An analytical digital balance (Scientech, SA210) with a precision of 0.1 mg was used to determine the specimen mass, while Archimedes' principle was used to determine the sample volume.

III. COMPUTATIONAL AND EXPERIMENTAL RESULTS

A. *CALPHAD Modeling*

Alloy screening was carried out at equi-molar compositions for simplicity. The phase mole fraction *vs* temperature plots using TCNi7 database suggest the possibility of forming HCP HEAs for six compositions, namely CoFeReRu, CoPtReRu, CoReRuV, CoCrReRu, CoCrFeReRu, and CoFeReRuV, as shown in Figure 1. Since the database only covers very limited numbers of the constituent ternaries for the compositions studied, the screening results should not be overestimated and are subject to experimental verification. The predicted liquidus temperature for CoFeReRu is 2237 K (1964 °C), and its solidus temperature is 1894 K (1621 °C). At $T \leq 824$ K (551 °C), a (Fe,Co)-rich B2 phase will precipitate, but due to the slow diffusion kinetics at this temperature, this precipitation reaction is expected to be very sluggish. The predicted compositions at 773 K (500 °C) are listed in Table I.

The HCP phase is predicted to be stable between 579 K (306 °C) and 2089 K (1816 °C) in CoPtReRu. The calculated liquidus temperature is 2388 K (2115 °C). An FCC phase will precipitate at $T \leq 579$ K (306 °C), but again this reaction is unlikely to occur due to kinetics freezing. For CoReRuV, the predicted liquidus temperature is 2189 K (1916 °C), and all the liquid transforms to the HCP phase at the solidus temperature of 1951 K (1678 °C). At $T \leq 909$ K (636 °C), a V-rich BCC phase will precipitate. For CoCrReRu, the predicted liquidus temperature is 2214 K (1941 °C), and the HCP phase is stable at a narrow temperature window of 1380 K to 1907 K (1107 °C to 1634 °C). The HCP phase is predicted to be stable at 998 K to 1763 K (725 °C to 1490 °C) and 978 K to 1700 K (705 °C to 1427 °C) for CoCrFeReRu and CoFeReRuV, respectively. The predicted liquidus temperature is 2075 K (1802 °C) for CoCrFeReRu and 2027 K (1754 °C) for CoFeReRuV.

B. *AIMD Simulations*

Only the partial PDFs of three representative HCP HEAs are presented in Figure 2, namely DyGdLuTbY, CoOsReRu, and MoPdRhRu. They represent those compositions that comprise rare earth elements with the HCP structure, transition metal elements with large terminal HCP solid solution, and transition metal elements that form intermediate HCP solid solution in the middle of their binary phase diagrams. Using SSOL5 database, the liquidus temperatures (T_{liq}) of these three alloys were predicted to be 1724 K, 2901 K, and 2168 K (1451 °C, 2628 °C, and 1895 °C), and the ratio of simulation temperatures (T_{sim}) over T_{liq} are 1.20, 1.06, and 1.42 for DyGdLuTbY, CoOsReRu, and MoPdRhRu, respectively.

Table I. Predicted Equilibrium Phase Compositions (Atomic Percent) on CoFeReRu at 773 K (500 °C)

Phase	Co	Fe	Re	Ru
HCP	23.2	22.6	27.1	27.1
BCC	45.9	53.6	0.3	0.2

As expected, all the first-nearest-neighbor partial PDFs for DyGdLuTbY have little variation in the peak intensity and the pair distance. As for CoOsReRu, the first-nearest-neighbor PDFs seem very uniform except that g_{CoCo} and g_{ReRe} are slightly lower in peak intensity. As for MoPdRhRu, the peak intensities are also comparable for all pairs except the Mo-Mo pair. The peak value of g_{MoMo} is noticeably lower than the other pairs, suggesting that Mo prefers to bond with Pd, Rh, or Ru than itself. The AIMD simulation results suggest the lack of strong chemical order or segregation in DyGdLuTbY and CoOsReRu, while the Mo-Mo pair distribution is lower in MoPdRhRu.

The MSD plots for these three alloys are linear as shown in Figure 3 (for clarity only the plots up to 8 ps are shown), and the diffusion constants (D_o) determined using Eq. [2] from the data within the time frame of 0.5 to 5 ps are listed in Table II. To describe the variation in diffusion constants, a parameter ΔD_o (in percentage) is defined as

$$\Delta D_o = \left| D_o^{max} - D_o^{min} \right| / D_o^{min}, \qquad [3]$$

where D_o^{max} and D_o^{min} are the maximum and minimum diffusion constants among all the constituent elements, respectively. The calculated ΔD_o values are 8, 27, and 11 pct for DyGdLuTbY, CoOsReRu, and MoPdRhRu, respectively. The variations in D_o are relatively small, agreeing with the guidelines for searching new HEAs suggested in Reference 3 that emphasizes equivalent or comparable diffusivity among principal elements. Among these three alloys, the difference in the atomic radius is the most significant for CoOsReRu. Cobalt has the smallest atomic radius of 1.25 Å, while Re has the largest atomic radius of 1.38 Å. As a result, D_o is the largest for Co and smallest for Re in the alloy. For the other two alloys, the atomic radii are fairly close for the constituent elements, and as a result the variation in D_o is small. Note that at 3073 K (2800 °C), D_o for Ru in MoPdRhRu is 79 pct higher than Ru in CoOsReRu. This suggests that alloy chemistry impacts the diffusion constants greatly. The other reason why D_o values in CoOsReRu are much lower than those in MoPdRhRu could be because the T_{sim}/T_{liq} ratio is significantly lower for CoOsReRu than MoPdRhRu. It is generally anticipated that the tendency in chemical short-range order decreases with increasing the T_{sim}/T_{liq} ratio.

C. *Experimental Validation*

The as-cast CoFeReRu shows essentially a single HCP phase based on the BSE micrograph and XRD pattern, as shown in Figure 4. The lattice constants of the HCP phase are determined to be $a = 2.65$ Å and $c = 4.19$ Å from the XRD pattern, and the axial ratio (c/a) is 1.58, which is very close to the ideal c/a ratio of 1.633 for the HCP lattice. The dendritic microstructure and the contrast in the BSE micrograph indicate

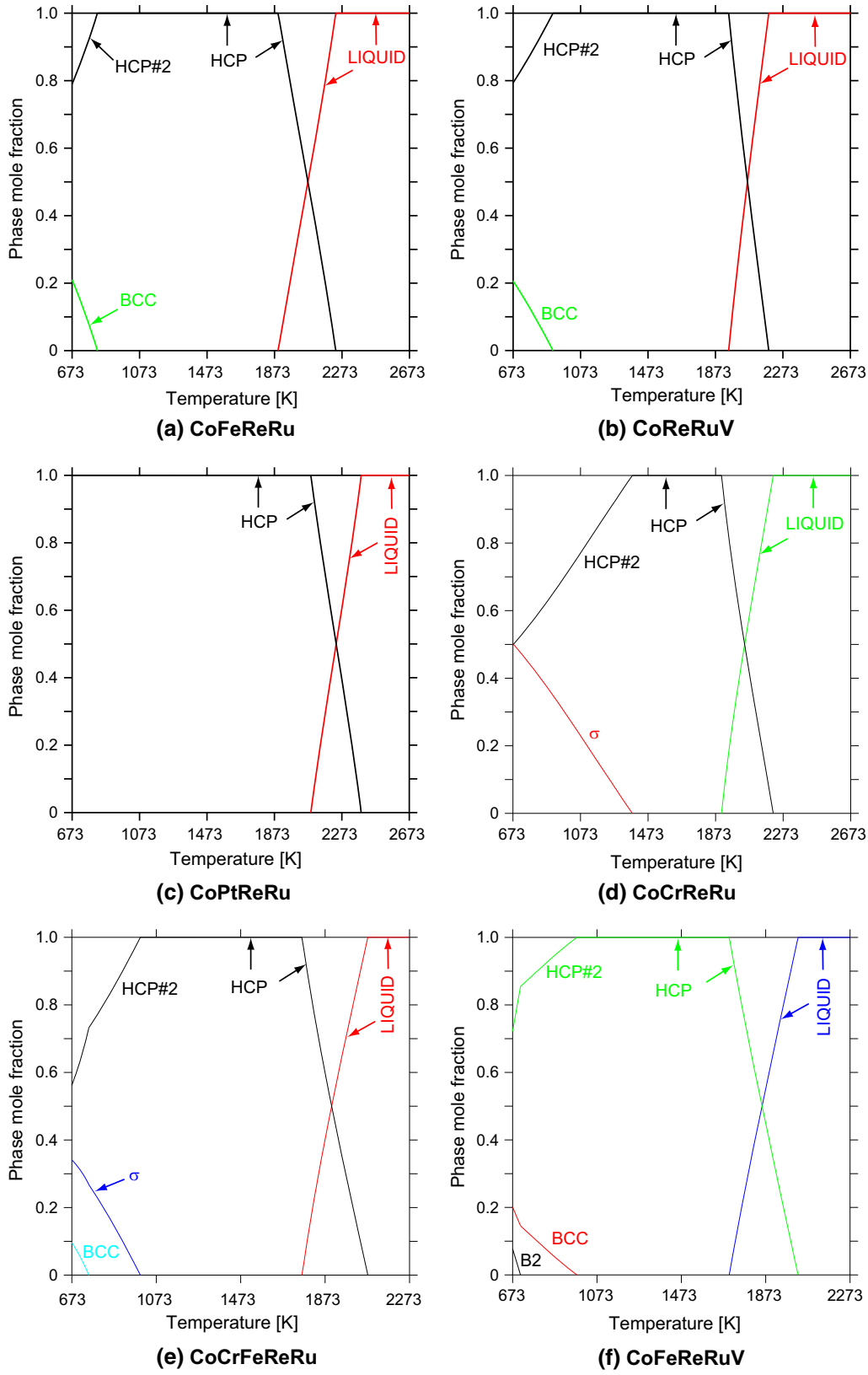

Fig. 1—Equilibrium phase mole fraction *vs* temperature for CoFeReRu, CoReRuV, CoCrReRu, CoPtReRu, CoCrFeReRu, and CoFeReRuV predicted from TCNI7 database.

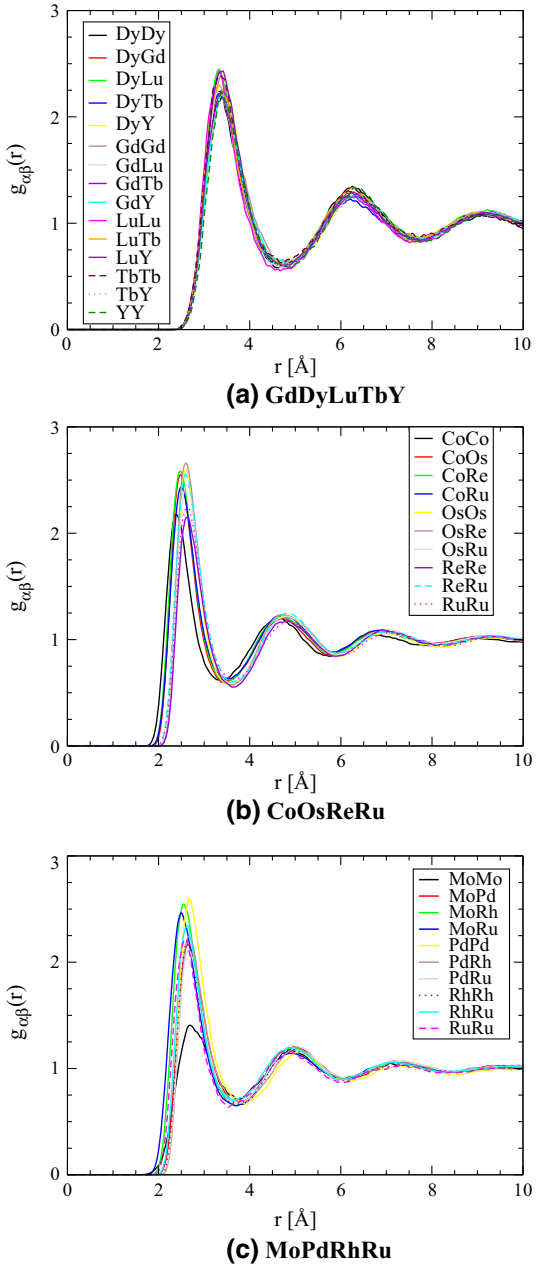

Fig. 2—Partial pair distribution functions predicted from AIMD simulations.

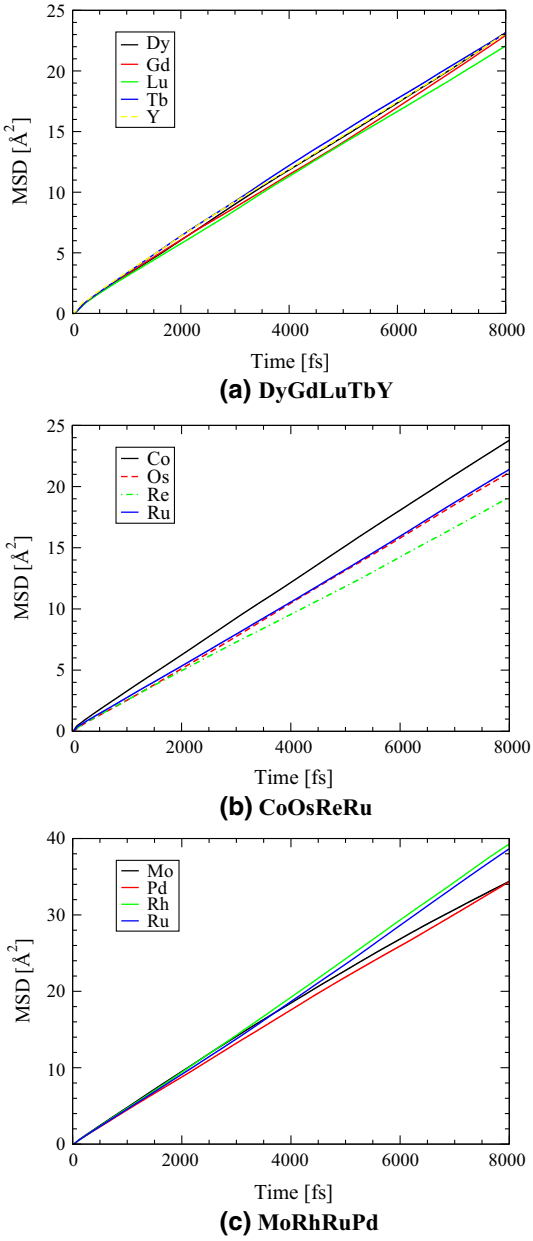

Fig. 3—Mean square displacement *vs* time plots predicted from AIMD simulations.

compositional segregation which are displayed in Figure 5. Dendrites form first during solidification and are enriched in Re followed by Ru. Cobalt and Fe are rejected to the liquid and are enriched in the interdendritic regions that form at later stages.

In contrast, the presence of an HCP phase and an unknown phase(s) is detected in the as-cast CoReRuV shown in Figure 6. A typical dendritic microstructure forms. The HCP phase is confirmed in the XRD by arithmetical manipulation of the observed $\sin^2\theta$ values in an attempt to find certain relationships among them. The lattice constants are determined to be $a = 2.69$ Å, $c = 4.32$ Å, and $c/a = 1.606$. These values are very close to the lattice parameters of Ru or HCP Ru-Co alloys.[22] Due to peak overlapping in XRD, the crystal structure pertaining to the remaining peaks cannot be identified exactly, and other advanced characterization tools such as transmission electron microscopy (TEM) will be needed to provide more conclusive and complementary information on the microstructure.

IV. DISCUSSION

A. *Searching Strategies*

Inspection of binary and ternary phase diagrams can provide useful guidance on proper combination of elements in forming solid solutions,[5] but it is not

Table II. Diffusion Constants for DyGdLuTbY, CoOsReRu, and MoPdRhRu Obtained from AIMD Simulations

Alloys	T_{sim} [K (°C)]	T_{liq} [K (°C)]	Diffusion Constant ($\times 10^{-5}$ cm^2/s)				
			*A***	*B***	*C***	*D***	*E***
DyGdLuTbY	2073 (1800)	1724 (1451)	4.84 ± 0.05	4.56 ± 0.04	4.57 ± 0.04	4.91 ± 0.04	4.76 ± 0.09
CoOsReRu	3073 (2800)	2901 (2628)	4.95 ± 0.01	4.40 ± 0.04	3.90 ± 0.04	4.34 ± 0.02	
MoPdRhRu	3073 (2800)	2168 (1895)	7.60 ± 0.11	7.28 ± 0.01	8.08 ± 0.07	7.79 ± 0.11	

T_{sim} refers to the simulation temperature, and T_{liq} is the calculated liquidus temperature.
***A*, *B*, *C*, *D*, and *E* refer to the elements in the alloys in alphabetical order.

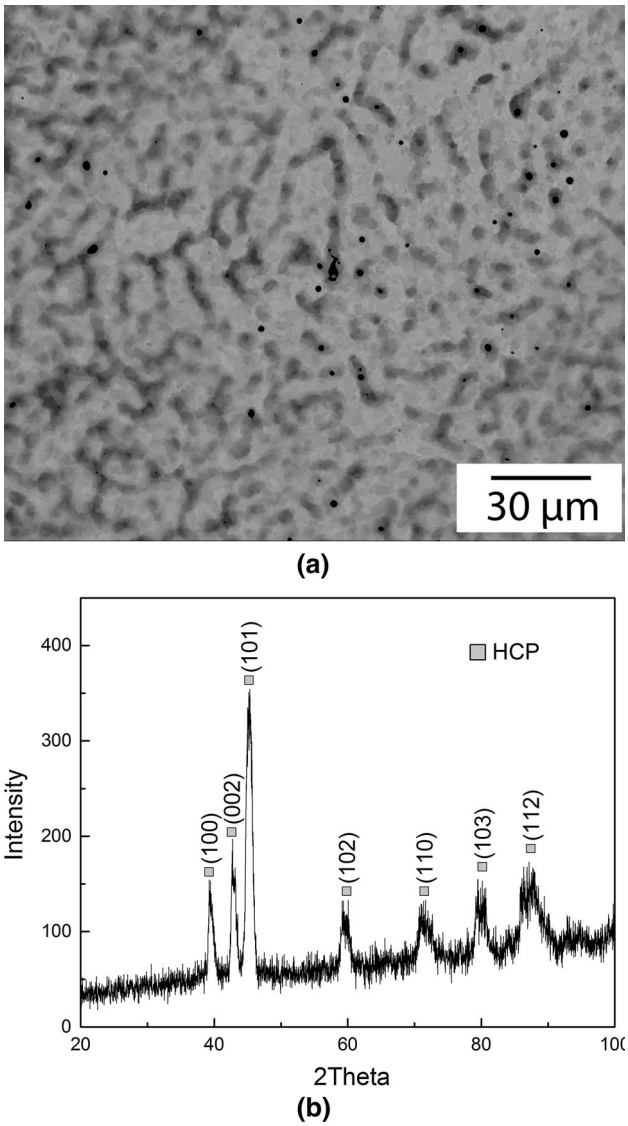

Fig. 4—(*a*) BSE micrograph and (*b*) XRD pattern of CoFeReRu in the as-cast state.

known exactly how the edge binaries will extend into ternaries, how ternaries will extend into quaternaries, and so on. The phase relationship in a multi-component system can be very complex as a function of temperature and composition. Mind that TCNI7 database does not cover some key elements such as Tc, Rh, and Ir that are important to forming HCP HEAs, so one has to rely on experimental phase diagrams to start initial screening pertaining to these elements. The CALPHAD approach not only helps visualize phase diagrams, but also greatly accelerate HEA design *via* extrapolation from constituent binaries and ternaries. The accuracy of the extrapolation method critically relies on the validity of the Gibbs free energy description for the constituent binaries and ternaries as well as those hypothetical phases that are required for sublattice compatibility purpose, as stated in a recent comprehensive review on CALPHAD modeling of HEAs.[33] On the other hand, AIMD simulations will provide quantitative information on preferred interatomic interactions without experimental input and can be used to assist searching for new HEAs.[3,5] The present AIMD simulations on DyGdLuTbY, CoOsReRu, and MoPdRhRu (Figure 2) and other compositions (not shown) suggest the lack of potent short-range order in these alloys, and this usually promotes solid solution formation as has been pointed out in References 3, 5.

Out of six compositions (Figure 1) predicted to be HCP HEAs by TCNI7 database, experimental verification was carried out on CoFeReRu and CoReRuV. Both XRD and SEM analyses confirmed that the as-cast CoFeReRu has the HCP crystal structure, while more than one phase was present in CoReRuV. Ruthenium can dissolve up to 73 at. pct Fe at 673 K (400 °C) in Fe-Ru binary,[22] while at least three stable intermetallic compounds form in Fe-Re binary. The isomorphous FCC solid solution forms in Co-Fe binary system.[22] Formation of single HCP phase in CoFeReRu indicates that the impressively large Fe solubility in Ru outweighs the competing Fe-Re compounds and the FCC phase in Co-Fe binary in terms of phase stability.

In contrast, several stable compounds form in Re-V and Co-V binaries,[22] and both HCP Co and Re have little solubility for V.[22] For Re-V binary, a σ phase VRe_3 (prototype CrFe, Pearson symbol tP30, space group $P4_2/mnm$) forms at 2243 K to 2733 K (1970 °C to 2460 °C), and a Cr_3Si type phase (Pearson symbol cP8, space group $Pm\bar{3}m$) forms at 1743 K to 2553 K (1470 °C to 2280 °C). At 1073 K (800 °C), V has over 55 at. pct solubility for Re, but Re has less than 3 at. pct solubility for V. For Ru-V system, Ru has fairly large solubility of 16 at. pct V at 873 K (600 °C), and V has very large solubility for Re although the B2 phase with wide compositional homogeneity range exists at 873 K (600 °C). For Co-V system, the mutual

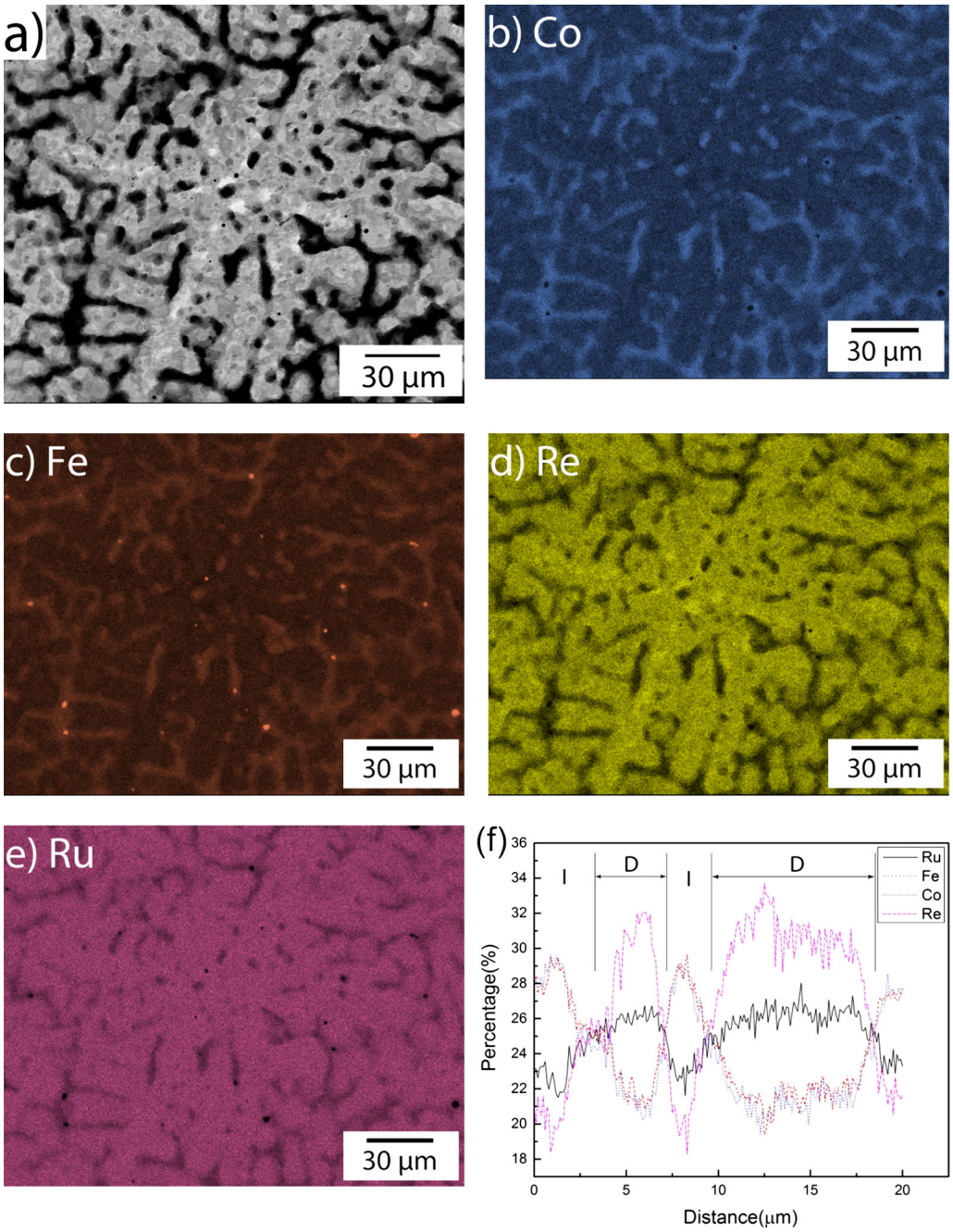

Fig. 5—Microsegregation in the as-cast CoFeReRu: (*a*) BSE image, elemental distribution of (*b*) Co, (*c*) Fe, (*d*) Re, and (*e*) Ru, and (*f*) line scan. "D" signifies dendrite regions and "I" interdendritic regions.

solubility is low at lower temperatures, and three compounds form Co_3V (prototype $PuAl_3$, hP24, space group $P6_3/mmc$) below 1329 K (1056 °C); the $Co_{0.4}V_{0.6}$ σ phase forms with wide compositional homogeneity range at 518 K to 1692 K (245 °C to 1419 °C); and CoV_3 (prototype Cr_3Si, cP8) forms at $T \leq 1303$ K (1030 °C). In short, the binary phase diagrams hint that an addition of V to CoReRu may destabilize the HCP phase, and this agrees with the present experimental observation.

The disagreement on phase stability in CoReRuV between CALPHAD prediction and experiments demonstrates the importance of the reliability of the thermodynamic database. The lack of thermodynamic descriptions for the constituent ternaries is assumed to be mainly responsible for the disagreement. For the same reason as CoReRuV, it is unlikely that CoFeReRuV would form single-phase HCP structure in the as-cast state. While Ru can dissolve up to 41 at. pct Cr at 773 K (500 °C), the σ phase is also stable in both

Co-Cr and Cr-Re binaries. On the other hand, whether TCNI7 database overestimates the thermodynamic stability of the HCP solid solution over the σ phase (as shown in Figure 1) for CoCrReRu and CoCrFeReRu is not readily known. As for CoPtReRu, Re can dissolve up to 40 at. pct Pt at 1073 K (800 °C) in Pt-Re system,[22] and Ru can dissolve 20 at. pct Pt at 1273 K (1000 °C) in Pt-Ru system,[22] while an isomorphous FCC solid solution forms in Co-Pt system.[22] Future research will focus on the phase relationship in CoCrReRu, CoCrFeReRu, and CoPtReRu. In summary, due to lack of experimental phase diagrams on ternary and higher-order systems, the efficient searching strategy[5] by combining phase diagram inspection, CALPHAD modeling, and AIMD simulations can accelerate HEA design, while experimental verification is always important.

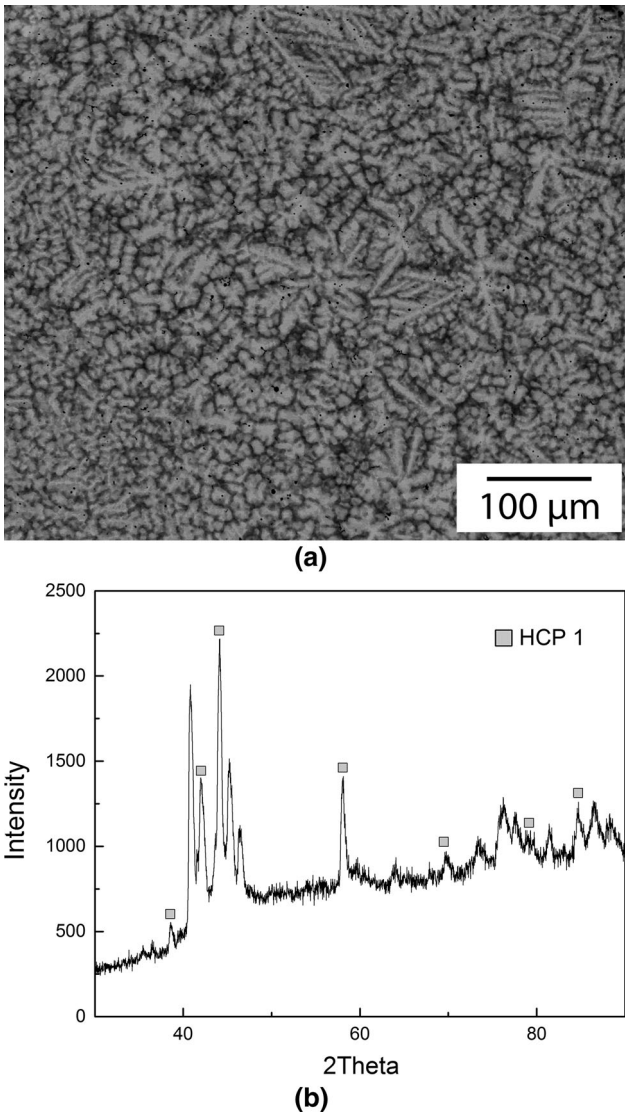

Fig. 6—(*a*) BSE micrograph and (*b*) XRD pattern of CoReRuV in the as-cast state. Those unlabelled peaks in XRD are from unknown phase(s).

B. *HCP HEAs Based on Rare Earth Elements*

Based on the binary phase diagram information, it is tempting to propose that arbitrary mixing of the following ten elements in a variety of molar ratios will favor formation of single-phase HCP structures: Sc, Y, Sm, Gd, Tb, Dy, Ho, Er, Tb, and Lu (ranked as type I in Table III). Since several of these elements transform to the BCC structure at very high temperatures before melting, some of the HEAs that comprise these elements may require subsequent annealing in the HCP phase field in order to decompose the primary BCC phase, if any should exist. In other words, the XRD pattern for some of these alloys in the as-cast condition may contain the BCC phase.

Out of these ten elements (type I in Table III), the total number of equi-molar compositions that may form single-phase HCP HEAs is 974, determined as follows:

$$C_{10}^{4} + C_{10}^{5} + C_{10}^{6} + C_{10}^{7} + C_{10}^{8} + C_{10}^{9} + C_{10}^{10} = 210 + 378 + 210 + 120 + 45 + 10 + 1. \quad [4]$$

The individual item in Eq. [4] represents the total number of compositions for quaternary, quinary, senary, septenary, octonary, ennead, and decadal systems, respectively.

Early rare earth elements La, Ce, Pr, Nd, and Pm (ranked as type II in Table III) all have a stable DHCP structure at lower temperatures, and they all form isomorphous DHCP solid solution in their binary systems.[22] Therefore, formation of single DHCP phase is anticipated in CeLaNdPmPr, CeNdPmPr, CeLaPmPr, CeLaNdPr, CeLaNdPm, and LaNdPmPr.

Since most of the type I HCP elements have large solubility for type II DHCP elements, it is still possible to form single-phase HCP solid solution based on type I elements ($N \geq 4$) with the addition of one or two type II elements at equal, or near-equal, molar ratio. In this case, it will be interesting to see if the HCP solid solution will destabilize the binary compound (prototype LaY, Pearson symbol hR9, Space group $R\bar{3}m$) that is observed in the binary phase diagrams that comprise type I and type II elements. It is unlikely that including Eu and/or Yb as principal elements will help HCP HEA formation since both are nearly insoluble in those HCP/DHCP rare earth elements mentioned above. Europium

Table III. Ranking of Rare Elements in Forming HCP HEAs

Type	Lattice	Elements									
I	HCP	Sc	Y	Sm	Gd	Tb	Dy	Ho	Er	Tm	Lu
II	DHCP	La	Ce	Pr	Nd	Pm					

Table IV. Classification of HCP HEAs Based on Transition Metals

Type	Comment	Alloy Compositions
I	isomorphous	CoOsReRu, CoFeReRu, CoCrReRu, CoPtReRu, CoCrFeReRu, CoOsReRuX, X = Fe, Tc, Pd, Pt, Rh, Ir, Ni or their combination
	large solubility	$(Cr,Mo)_{0.5}(OsRu)_{0.5}$, $(Cr,W)_{0.5}(OsRu)_{0.5}$, $(Mo,W)_{0.5}(OsRu)_{0.5}$, $(Cr,Mo,W)_{0.5}(OsRu)_{0.5}$, and CrMoOsRuW
II	intermediate	CrIrMoRh, CrIrRhW, IrMoRhW, $(Cr,Mo,W)_{0.5}(IrRh)_{0.5}$, CrIrMoRhW, MoPdRhRu, MoPtRhRu, IrMoPdRu, IrMoPtRu, IrMoPtRhRu, and IrMoPdPtRhRu.

has a stable BCC structure below its melting point of 1095 K (822 °C), and Yb has a stable FCC structure below its melting point of 1092 K (819 °C).

C. *HCP HEAs Based on Transition Metal Elements*

There are two scenarios where the HCP phase appears in binary phase diagrams: One is the extension of the terminal HCP phase into the center of the phase diagram such as those based on rare earth elements addressed in Section IV–A and CoOsReRu.[5] For CoOsReRu, all six constituent binary systems form complete isomorphous solid solution, and no stable intermetallics are observed. Technetium, a radioactive element, has large terminal solubility in HCP lattice for Rh, Ir, Pd, and Ni, and it forms isomorphous solid solution with Re.

The other is intermediate HCP phase with varying amounts of compositional homogeneity ranges in the middle of a phase diagram, such as $Mo_{0.46}Pd_{0.54}$, $Mo_{0.4}Rh_{0.6}$, $Mo_{0.63}Ru_{0.37}$, *etc*. The MoPdRhRu HEA[34] belongs to this type. Chemical similarity between Pd and Pt and between Rh and Ir suggests that it is possible to form several HCP solid solution that are variants of MoPdRhRu, *e.g*., MoPtRhRu, IrMoPtRu, IrMoPtRhRu, and IrMoPdPtRhRu. Furthermore, a similar scenario is observed in binary systems of Cr/Mo/W with Ir/Rh. For example, the HCP $Cr_{0.5}Rh_{0.5}$ exhibits very wide compositional homogeneity range in the Cr-Rh binary.[22] In summary, those compositions that hold promise in forming HCP HEAs are listed in Table IV.

Although only equi-molar compositions are suggested in the present work, many more compositions at near equi-molar ratios or even very wide ranges of compositions may form single-phase HCP HEAs. On the other hand, it is also possible that not all the compositions recommended in Tables III and IV will form single-phase HCP solid solutions in the as-cast state; therefore, future experimental verification (including annealing at high temperatures to reach thermodynamic equilibrium) as well as theoretical studies[33,35–41] will be needed to identify suitable compositions.

V. CONCLUSIONS

Following the efficient searching strategy proposed in Reference 5, the present study focused on the design of single-phase HCP HEAs by combining phase diagram inspection, CALPHAD calculations, and AIMD simulations based on rare earth elements and transition metals. A series of alloy compositions that hold significant potential in forming single-phase HCP HEAs were identified. The following conclusions were drawn as a result:

1. Although six alloys were predicted to be single-phase HCP HEAs using TCNI7 database, the single HCP structure was experimentally confirmed in CoFeReRu using XRD and SEM while CoReReRuV contained more than one phase in the as-cast state. Also CoFeReReRuV may not form single-phase HEA. The disagreement between CALPHAD prediction and experiment is assumed mainly due to the absence of description for the constituent ternaries.
2. Formation of single-phase HCP structure is possible for CoCrReRu, CoCrFeReRu, and CoPtReRu, and future experiments to verify this are very desirable.
3. Most favorable rare earth elements to form HCP HEAs are Sc, Y, Sm, Gd, Tb, Dy, Ho, Er, Tm, and Lu. There could be a total of 974 equi-molar alloys with 4 to 10 principal components. Addition of one or two principal DHCP elements of La, Ce, Pr, Nb, or Pm is possible without causing formation of other phases.
4. It is likely that single DHCP phase will form in CeLaNdPmPr, CeNdPmPr, CeLaPmPr, CeLaNdPr, CeLaNdPm, and LaNdPmPr.
5. Those transition metals among which isomorphous solid solution prevails in edge binary or ternary systems promote forming HCP HEAs. They include CoOsReRu, CoFeReRu, CoCrReRu, CoPtReRu, CoCrFeReRu, and $Co_{0.2}Os_{0.2}Re_{0.2}Ru_{0.2}X_{0.2}$ (X = Fe, Tc, Pd, Pt, Rh, Ir, Ni, or their combinations).
6. Both Os and Ru have extensive solubility for Cr, Mo, or W, and thus it is likely that HCP solid solution may form in $(Cr,Mo)_{0.5}(OsRu)_{0.5}$, $(Cr,W)_{0.5}(OsRu)_{0.5}$, $(Mo,W)_{0.5}(OsRu)_{0.5}$, $(Cr,Mo,W)_{0.5}(OsRu)_{0.5}$, and even CrMoOsRuW.
7. The intermediate HCP phase with wide homogeneity range in the middle of binary phase diagrams (*e.g.,* Cr/Mo/W-Ir/Rh and Mo-Pd/Pt/Ir/Rh binaries) can extend into higher composition space to form single-phase HCP HEAs. They are CrIrMoRh, CrIrRhW, IrMoRhW, $(Cr,Mo,W)_{0.5}(IrRh)_{0.5}$, CrIrMoRhW, MoPdRhRu, MoPtRhRu, IrMoPdRu, IrMoPtRu, IrMoPtRhRu, and IrMoPdPtRhRu.
8. AIMD simulations show lack of strong chemical order or segregation in DyGdLuTbY, CoOsReRu,

and MoPdRhRu except that the Mo-Mo pair distribution is much lower in MoPdRhRu.

9. AIMD simulations show that the maximum variations in diffusion constants are 8, 27, and 11 pct for DyGdLuTbY, CoOsReRu, and MoPdRhRu at 2073 K, 3073 K, and 3073 K (1800 °C, 2800 °C, and 2800 °C), respectively. The larger variation for CoOsReRu is due to its larger difference in atomic radius among the components than the other alloys.

ACKNOWLEDGMENTS

This work was funded by the Cross-Cutting Technologies Program at the National Energy Technology Laboratory (NETL) – Strategic Center for Coal, managed by Robert Romanosky (Technology Manager) and Charles Miller (Technology Monitor). The Research was executed through NETL's Office of Research and Development's Innovative Process Technologies (IPT) Field Work Proposal. Research performed by AECOM Staff was conducted under the RES contract DE-FE-0004000. M.C.G. wishes to thank Mike Widom, Dan Sorescu, Bryan Morreale, and David Alman for useful discussions on the HEA topic, and Paul Mason, Andreas Markström, and Qing Chen from ThermoCalc for technical support.

DISCLAIMER

REFERENCES

1. B. Cantor, I.T.H. Chang, P. Knight, and A.J.B. Vincent: *Mater. Sci. Eng. A*, 2004, vols. 375–377, pp. 213–18.
2. J.W. Yeh, S.K. Chen, S.J. Lin, J.Y. Gan, T.S. Chin, T.T. Shun, C.H. Tsau, and S.Y. Chang: *Adv. Eng. Mater.*, 2004, vol. 6, pp. 299–303.
3. Y. Zhang, T.T. Zuo, Z. Tang, M.C. Gao, K.A. Dahmen, P.K. Liaw, and Z.P. Lu: *Prog. Mat. Sci.*, 2014, vol. 61, pp. 1–93.
4. M.C. Gao, J.W. Yeh, P.K. Liaw, and Y. Zhang: *High-Entropy Alloys: Fundamentals and Applications*, Springer, Cham, 2015.
5. M.C. Gao and D.E. Alman: *Entropy*, 2013, vol. 15, pp. 4504–19.
6. F. Otto, Y. Yang, H. Bei, and E.P. George: *Acta Mater.*, 2013, vol. 61, pp. 2628–38.
7. L.J. Santodonato, Y. Zhang, M. Feygenson, C.M. Parish, M.C. Gao, R.J.K. Weber, J.C. Neuefeind, Z. Tang, and P.K. Liaw: *Nat. Commun.*, 2015, vol. 6, p. 5964.
8. Y. Zhang, S. Guo, C.T. Liu, and X. Yang: in *High-Entropy Alloys: Fundamentals and Applications*, M.C. Gao, J.W. Yeh, P.K. Liaw, and Y. Zhang, eds., Springer, Cham, 2015.
9. M.S. Lucas, G.B. Wilks, L. Mauger, J.A. Munoz, O.N. Senkov, E. Michel, J. Horwath, S.L. Semiatin, M.B. Stone, D.L. Abernathy, and E. Karapetrova: *Appl. Phys. Lett.*, 2012, vol. 100, pp. 251907-1–251907-4.
10. Z. Wu, H. Bei, F. Otto, G.M. Pharr, and E.P. George: *Intermetallics*, 2014, vol. 46, pp. 131–40.
11. C.J. Tong, Y.L. Chen, S.K. Chen, J.W. Yeh, T.T. Shun, C.H. Tsau, S.J. Lin, and S.Y. Chang: *Metall. Mater. Trans. A*, 2005, vol. 36A, pp. 881–93.
12. W.R. Wang, W.L. Wang, S.C. Wang, Y.C. Tsai, C.H. Lai, and J.W. Yeh: *Intermetallics*, 2012, vol. 26, pp. 44–51.
13. Z. Tang, M.C. Gao, H.Y. Diao, T.F. Yang, J.P. Liu, T.T. Zuo, Y. Zhang, Z.P. Lu, Y.Q. Cheng, Y.W. Zhang, K.A. Dahmen, P.K. Liaw, and T. Egami: *JOM*, 2013, vol. 65, pp. 1848–58.
14. S. Liu, M.C. Gao, P.K. Liaw, and Y. Zhang: *J. Alloys Compd.*, 2015, vol. 619, pp. 610–15.
15. O.N. Senkov, G.B. Wilks, D.B. Miracle, C.P. Chuang, and P.K. Liaw: *Intermetallics*, 2010, vol. 18, pp. 1758–65.
16. B. Zhang, M.C. Gao, Y. Zhang, S. Yang, and S.M. Guo: *Mater. Sci. Technol.*, 2015, vol. 31, pp. 1207–13.
17. H. Bei: USPC (UT-BATTELLE, LLC, Oak Ridge, TN: USA, 2013), US patent 20130108502 A1.
18. M.C. Gao, B. Zhang, S. Yang, and S.M. Guo: *Metall. Mater. Trans. A,* 2015, vol. submitted.
19. M.C. Gao, C.S. Carney, Ö.N. Doğan, P.D. Jablonksi, J.A. Hawk, and D.E. Alman: *JOM,* 2015, vol. submitted.
20. Y.L. Chen, C.W. Tsai, C.C. Juan, M.H. Chuang, J.W. Yeh, T.S. Chin, and S.K. Chen: *J. Alloys Compd.*, 2010, vol. 506, pp. 210–15.
21. K.M. Youssefa, A.J. Zaddach, C. Niu, D.L. Irving, and C.C. Koch: *Mater. Res. Lett.*, 2015, vol. 3, pp. 95–99.
22. H. Okamoto: *Desk Handbook: Phase Diagrams for Binary Alloys*, ASM International, Materials Park, OH, 2000.
23. M. Feuerbacher, M. Heidelmann, and C. Thomas: *Mater. Res. Lett.*, 2014, vol. 3, pp. 1–6.
24. A. Takeuchi, K. Amiya, T. Wada, K. Yubuta, and W. Zhang: *JOM*, 2014, vol. 66, pp. 1984–92.
25. B. Sundman, B. Jansson, and J.O. Andersson: *CALPHAD*, 1985, vol. 9, pp. 153–90.
26. G. Kresse and J. Hafner: *Phys. Rev. B*, 1993, vol. 47, pp. 558–61.
27. G. Kresse and J. Furthmüller: *Phys. Rev. B*, 1996, vol. 54, pp. 11169–86.
28. L. Verlet: *Phys. Rev.*, 1967, vol. 159, p. 98.
29. S. Nose: *J. Chem. Phys.*, 1984, vol. 81, pp. 511–19.
30. P.E. Blochl: *Phys. Rev. B*, 1994, vol. 50, pp. 17953–79.
31. J.P. Perdew, A. Ruzsinszky, G.I. Csonka, O.A. Vydrov, G.E. Scuseria, L.A. Constantin, X.L. Zhou, and K. Burke: *Phys. Rev. Lett.*, 2008, vol. 100, p. 136406.
32. P. Ganesh and M. Widom: *Phys. Rev. B*, 2008, vol. 77, p. 014205.
33. C. Zhang and M.C. Gao: in *High-Entropy Alloys: Fundamentals and Applications*, M.C. Gao, J.W. Yeh, P.K. Liaw, and Y. Zhang, eds., Springer, Cham, 2015.
34. J.O.A. Paschoal, H. Kleykamp, and F. Thummler: *Z. Metallkd.*, 1983, vol. 74, pp. 652–64.
35. M. Widom: in *High-Entropy Alloys: Fundamentals and Applications*, M.C. Gao, J.W. Yeh, P.K. Liaw, and Y. Zhang, eds., Springer, Cham, 2015.
36. M.C. Gao, C. Niu, C. Jiang, and D.L. Irving: in *High-Entropy Alloys: Fundamentals and Applications*, M.C. Gao, J.W. Yeh, P.K. Liaw, and Y. Zhang, eds., Springer, Cham, 2015.
37. M.C. Gao: in *High-Entropy Alloys: Fundamentals and Applications*, M.C. Gao, J.W. Yeh, P.K. Liaw, and Y. Zhang, eds., Springer, Cham, 2015.
38. M. Widom, W.P. Huhn, S. Maiti, and W. Steurer: *Metall. Mater. Trans. A*, 2014, vol. 45A, pp. 196–200.

39. M.C. Troparevsky, J.R. Morris, P.R.C. Kent, A.R. Lupini, and G.M. Stocks: *Phys. Rev. X*, 2015, vol. 5, p. 011041.
40. F.Y. Tian, L. Delczeg, N.X. Chen, L.K. Varga, J. Shen, and L. Vitos: *Phys. Rev. B*, 2013, vol. 88, p. 085128.
41. F. Tian, Y. Wang, D.L.L. Irving, and L. Vitos: in *High-Entropy Alloys: Fundamentals and Applications*, M.C. Gao, J.W. Yeh, P.K. Liaw, and Y. Zhang, eds., Springer, Cham, 2015.